# Surrogate methods for determining profiles of material properties of planar test objects with accumulation of apriori information about them

**Volodymyr Y. Halchenko** , **Ruslana Trembovetska** ,
**Volodymyr Tychkov** , **Nataliia Tychkova**

*Instrumentation, Mechatronics and Computer Technologies Department*
*Cherkasy State Technological University*
*Blvd. Shevchenka, 460, 18006, Cherkasy, Ukraine*

e-mail: *{v.halchenko/r.trembovetska/v.tychkov/n.b.tychkova.asp21}@chdtu.edu.ua*

**Abstract:** New methods for identifying the material properties of planar objects as a result of measurements by the eddy current method are proposed. The methods are based on the latest surrogate strategies and advanced optimization techniques that improve efficiency and reduce resource consumption of problem solutions, and balance computational complexity with the accuracy of the results. High-performance metamodels for global surrogate optimization are based on deep truly meaningful fully connected neural networks, serving as an additional function of accumulating apriori information about objects. High accuracy of the approximation of the multidimensional response surface, which is determined by the "exact" electrodynamic model of the testing process, is ensured by performing calculations according to the computer design of a homogeneous experiment with a low weighted symmetric centered discrepancy. The results of numerical experiments performed for full and reduced dimensional search spaces, which can be obtained by linear transformations using the principal component method, are presented. The verification of the methods proved their sufficiently high accuracy and computational performance.

**Key words:** accumulation of apriori information, electrical conductivity and magnetic permeability profiles, neural network metamodel, structuroscopy, surface eddy-current probe, surrogate optimization

# 1. Introduction

Structuroscopy is one of the most complex types of eddy-current non-destructive objects testing. It is aimed at determining the structure-dependent distributions of material properties, that is electrical conductivity (EC) and magnetic permeability (MP), along the depth of the material of objects [1,2], with the following conclusions about their structural features, namely the state of heat treatment and internal stress, hardness and temperature, etc. Hence, according to the measurement results of the amplitude and phase of the signals of eddy-current probes (ECP) caused by changes in the electromagnetic field as it passes through layers of the material with different properties and use of special algorithms for processing of the obtained data, the profiles of the and MP are reconstructed.

Most often, the inversion method and the method of the inverse measurement problem are used for this purpose, which in the vast majority of cases exploit optimization approaches to reproduce profiles [3], involving minimization of the difference between the results of calculations based on the mathematical model of field and material interaction and the measurements. The authors give an analytical review of various applications of this technique in [4], considered in the context of eddy-current measurements of profiles of material properties of cylindrical objects. However, due to their versatility, their use in relation to planar test objects (TO) is not a subject to fundamental limitations with the same inherent advantages and disadvantages. Therefore, in the authors' opinion it does not require a separate analysis. The authors in article [5] present an additional analysis of modern research on this problem. Moreover, we note a significant interest in these techniques for solving inverse problems, in the works [6–8]. The use of optimization algorithms and physical multi-frequency measurements by eddy-currents is common to them, which significantly complicates the implementation of the proposed approaches. The research [9–11] offers to carry out measurements with devices with complex circuitry at swept-frequency for the same purpose, leading to similar disadvantages as in the previous case. In [12] the authors' attention is, however, on the advantages of application of data-driven methods for the EC profiles assessment. However, the findings are characterized by low accuracy. The combination of the iterative inversion procedure, processing the results of experimental measurements with finite element data modelling, discussed in [13] for reconstructing the distribution, is hardly acceptable due to its significant computational resource intensity.

With this background, we must note that the features of ensuring accuracy when using the most common ones for such tasks of analytical mathematical models of the Uzal-Cheng-Dodd-Deeds type [5] for solving the problem of optimization techniques require a significant number of the desired variables, which together determine the EC and MP profiles. Their number for complex and realistic problems of profiles reproduction is hundreds, leading to a significant increase in computational resource consumption. Proxy-modelling is a way out of this situation. The role of a proxy-model can be played by a neural network metamodel, which, on the one hand, provides a significant reduction in resource consumption, and on the other hand, acts as a carrier of previously accumulated information about the TO [14]. Such apriori information can be obtained due to numerical modelling using an electrodynamic model of the eddy-current testing process to increase information on changes in the material properties of an object during its multifrequency sounding, changes in the clearance between the ECP and the object, the depth of field penetration, etc. This metamodel application in the target function for reconstructing

profiles in the process of surrogate optimization significantly improves the resource consumption indicators when solving inverse problems, hence making them efficient. The same goal is achieved by a considerable reduction in the dimensionality of the latent search space during optimization, achieved by appropriate methods of its transformation.

Thus, **the aim of this research** is to develop methods for solving inverse problems of simultaneous reconstruction of profiles of material properties of objects in eddy-current measurements based on apriori information accumulation, the latest surrogate strategies, and advanced optimization techniques. This is certain to provide an improved efficiency and reduced resource consumption of solutions as well as balance between computational complexity and accuracy of results.

## 2. Formulation

In this research, we consider the process of eddy-current testing of planar objects performed with the use of ECPs surface (Fig. 1).
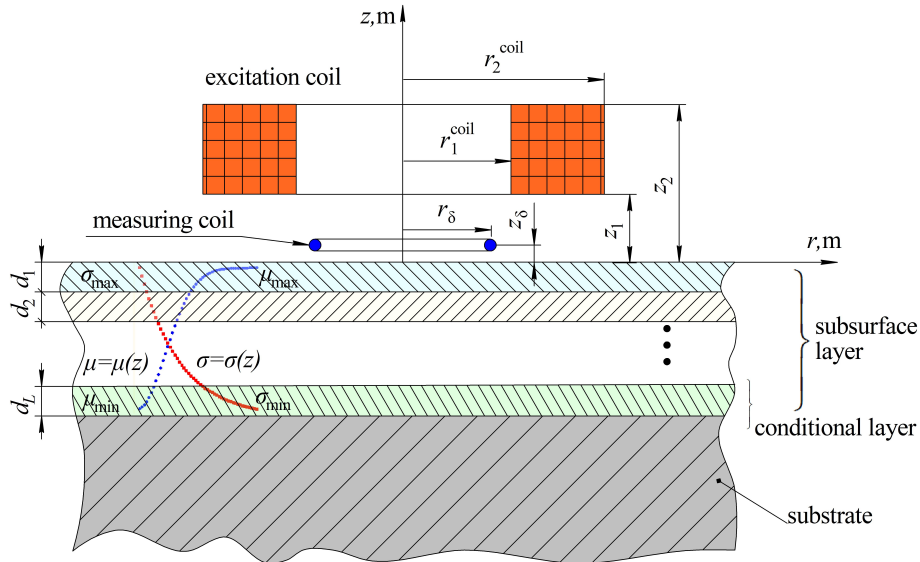


Fig. 1. Eddy-current measurement of EC and MP profiles of planar test objects

The objects are characterized by infinite overall dimensions. The determination of the EC and MP profiles is performed by numerical calculations based on the measured data. The algorithm for solving inverse problem involves the use of an electrodynamic model of the eddy-current testing process. To simplify it a subsurface TO layer with certain structural features caused, for example, by technological operations to strengthen its surface is considered conditionally multi-layered. Moreover, each of the conditional layers is characterized by different piecewise constant values of material properties. The simulation of the continuity of EC and MP profiles is provided by a significant number of conditional layers $L$, which is generally considered to be quite significant.

The objects environment is assumed to be linear, homogeneous and isotropic. The electromagnetic field is excited by the EC a generator coil with a sinusoidal current $I$ varying with an angular frequency $\omega = 2 \cdot \pi \cdot f$. The model takes into account that the coil has a rectangular cross-section with finite dimensions, is characterized by a uniform current density across the cross-section $j_0$ and has a number of turns $W$. These assumptions are inherent in the analytical electrodynamic model Uzal-Cheng-Dodd-Deeds [15–18] of the eddy-current testing of planar TO, which for arbitrary number of conditional layers will later be used in the matrix form of writing in the Theodoulidis interpretation [19]. The output signal of the eddy current probe induced in the measuring coil of the ECP is calculated by the equation:

$$e_{\mathrm{mod}} = -j \cdot \omega \cdot w_{\mathrm{mes}} \cdot \oint_{Lc} A(P)\mathrm{d}l_p, \tag{1}$$

where: $A(P)$ is the azimuthal component of the magnetic vector potential at the observation point $P$, Wb/m; $w_{\mathrm{mes}}$ is the number of turns of the ECP measuring coil; $Lc$ is the contour of the measuring coil.

In turn, the magnetic vector potential at the observation point $P$ with coordinates $(r_\delta, z_\delta)$ is calculated in accordance with the equation:

$$A(r_\delta, z_\delta) = \int_0^\infty J_1(\kappa r_\delta) \cdot [C_s \cdot e^{\kappa z_\delta} + D_{ec} \cdot e^{-\kappa z_\delta}]\mathrm{d}\kappa, \tag{2}$$

where:

$$C_s = \frac{\mu_0 \cdot j_0}{2} \cdot \frac{\chi(\kappa r_1, \kappa r_2)}{\kappa^3} \cdot (e^{-\kappa z_1} - e^{-\kappa z_2}),$$

$$D_{ec} = \frac{(\kappa \cdot \mu_{t+1} - \lambda_1) \cdot V_{11}(1) + (\kappa \cdot \mu_{t+1} + \lambda_1) \cdot V_{21}(1)}{(\kappa \cdot \mu_{t+1} + \lambda_1) \cdot V_{11}(1) + (\kappa \cdot \mu_{t+1} - \lambda_1) \cdot V_{21}(1)} \cdot C_s,$$

$$j_0 = W \cdot I(r_2 - r_1)^{-1} \cdot (z_2 - z_1)^{-1},$$

$$\chi(x_1, x_2) = \left\{ x_1 \cdot J_0(x_1) - 2 \cdot \sum_{m=0}^\infty J_{2m+1}(x_1) \right\} - \left\{ x_2 \cdot J_0(x_2) - 2 \cdot \sum_{m=0}^\infty J_{2m+1}(x_2) \right\},$$

$$V(1) = T(1,2) \cdot T(2,3) \ldots T(L-2, L-1) \cdot T(L-1, L),$$

$$T_{11}(t, t+1) = \frac{1}{2} \cdot e^{(-\lambda_{t+1} + \lambda_t)\mathrm{d}t} \cdot \left( 1 + \frac{\mu_t}{\mu_{t+1}} \cdot \frac{\lambda_{t+1}}{\lambda_t} \right),$$

$$T_{12}(t, t+1) = \frac{1}{2} \cdot e^{(\lambda_{t+1} + \lambda_t)\mathrm{d}t} \cdot \left( 1 - \frac{\mu_t}{\mu_{t+1}} \cdot \frac{\lambda_{t+1}}{\lambda_t} \right),$$

$$T_{21}(t, t+1) = \frac{1}{2} \cdot e^{(-\lambda_{t+1} - \lambda_t)\mathrm{d}t} \cdot \left( 1 - \frac{\mu_t}{\mu_{t+1}} \cdot \frac{\lambda_{t+1}}{\lambda_t} \right),$$

$$T_{22}(t, t+1) = \frac{1}{2} \cdot e^{(\lambda_{t+1} - \lambda_t)\mathrm{d}t} \cdot \left( 1 + \frac{\mu_t}{\mu_{t+1}} \cdot \frac{\lambda_{t+1}}{\lambda_t} \right),$$

$$\lambda_t = \left( \kappa^2 + j \cdot \omega \cdot \mu_0 \cdot \mu_t \cdot \sigma_t \right)^{\frac{1}{2}}.$$

$V(1)$ is the matrix whose elements are $V_{11}$, $V_{21}$; $T()$ is the matrix with elements $T_{11}()$, $T_{12}()$, $T_{21}()$, $T_{22}()$; $\mu_0 = 4 \cdot \pi \cdot 10^{-7}$ is the magnetic constant in vacuum, H/m; $J_0()$, $J_1()$, $J_m()$ are the cylindrical Bessel functions of the first kind of zero, first, and $m$−th orders; $(r_2 - r_1)$ is the width of the cross-section of the ECP excitation coil, m; $(z_2 - z_1)$ is the height of the cross-section of the ECP excitation coil, m.

Based on this model (1), the authors created a software product that allows calculating the output signal of a surface probe under various measurement conditions, which has been thoroughly verified. The testing was carried out both by comparing with the calculations based on analytical models obtained for one- and two-layer TO [20] and the results of numerical calculations by the finite element method in the COMSOL Multiphysics (AC/DC Module) environment for a three-layer object [5], where the maximum relative error in determining the vector potential in terms of amplitude did not exceed 0.2% and in terms of phase –0.5%.

Thus, after the procedure of ECP measuring over a planar object, the signal amplitude and phase are subject to fixation according to one of the classical measurement designs [1]. Mathematically, the measured signal $e_{\text{mes}}$ can be represented in an algebraic form as the expression $e_{\text{mes}} = C_{\text{mes}} + j \cdot D_{\text{mes}}$, where $C_{\text{mes}}$ and $D_{\text{mes}}$ are its real and imaginary parts, respectively. Such a mathematical form of EMF representation allows for the further efficient creation of the target function $F$ to find the optimal values of the desired model parameters. Then, the task of reconstructing the EC and MP profiles is to minimize the following quadratic function:

$$F(\boldsymbol{\sigma}, \boldsymbol{\mu}, f, \ldots) = (C_{\text{mes}} - G_{\text{metamod}})^2 + (D_{\text{mes}} - Z_{\text{metamod}})^2 \rightarrow \min, \tag{3}$$

where: $e_{\text{metamod}} = G_{\text{metamod}} + j \cdot Z_{\text{metamod}}$ is the EMF value calculated using a neural network proxy-model (metamodel) on the electrodynamic model; $\boldsymbol{\sigma}, \boldsymbol{\mu}$ are the corresponding vectors of material properties determining the desired profiles.

## 3. Methodology

The main idea of this research is to use certain strategies and techniques of surrogate modelling in the optimization algorithm for finding profiles of material properties [21–24], ensuring a significant reduction in the resource consumption of problem solving and maintain a balance between its computational complexity and the accuracy of the results. The aim of this research has led to specific tasks, namely, the application of two approaches to the implementation of surrogate optimization techniques in inverse profile measurement problems.

The first (Fig. 2) is to create a high-performance metamodel in the search space, the dimensionality of which is determined by the summation of the dimensions of the vectors $\boldsymbol{\sigma}$ and $\boldsymbol{\mu}$.

The neural network metamodel is used in the design of the target function for calculating the EMF instead of the "computationally heavy" electrodynamic model $e_{\text{mod}}$. Given that, the dimensionality of the vectors $\boldsymbol{\sigma}$ and $\boldsymbol{\mu}$ is the same and equal to the number of conditional layers of the TO, the dimensionality of the space is equal to twice its value of one of these vectors. Since the number of conditional layers must be sufficiently large for the reasons mentioned earlier, the dimensionality of the search space is also appropriate. Consequently, the number of variables to be searched when implementing the optimization algorithm is significant, which complicates its implementation.
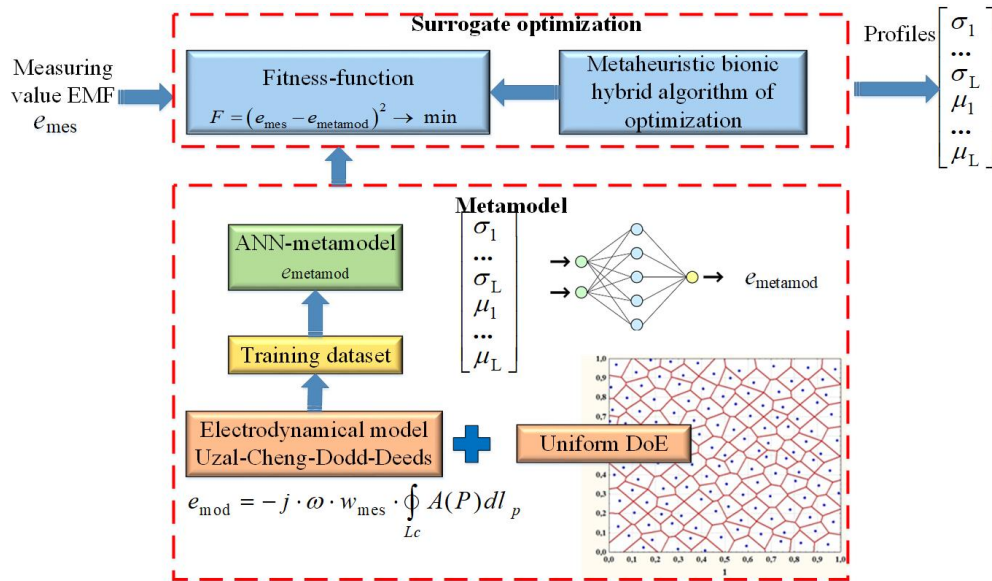
Fig. 2. General scheme of implementation of the classical surrogate optimization method for solving the inverse problem of MP and EC profiles determining

A feature of the metamodel is also its implementation in the form of two real-valued deep fully-connected neural networks (DFCNN) with common inputs, the outputs of which, when trained, take the values of the real and imaginary parts of the EMF $e_{\text{metamod}}$. This technique allows achieving much better results in the accuracy of the electrodynamic model approximation than when using the amplitude and phase of the ECP signal. The use of deep neural networks is due to their ability to detect complex nonlinear hierarchical dependencies between input and output data. Training, cross-validation, and test samples for creating metamodels are formed on the basis of a computer homogeneous design of the experiment (DOE) with low discrepancies rates [25–27], which ensures reliable reproduction of the multidimensional response surface during approximation. In addition to the usual function of high-performance computing for surrogate optimization, metamodels additionally perform the functions of apriori accumulation of information about the TO.

This effect is achieved by modelling in accordance with the DOE using an electrodynamic model as a result of varying material properties, excitation frequency, air clearance between the object and the ECP, etc. Consequently, all the above sample types with high-quality and diverse data are generated, which is crucial for neural network training. Finally, to find the extremum of the target function, a heuristic stochastic global optimization algorithm is used, namely a hybrid multi-agent particle swarm optimization algorithm with evolutionary formation of the swarm composition [28–30]. It is a kind of low-level hybridization of the particle swarm method with a genetic algorithm. This combination of algorithms has a positive effect on both the accuracy and speed of finding a global solution. The integration of algorithms allows finding the extremum for complex, including ravine-like, response surface topologies. Such surfaces are characteristic of

inverse problems that are considered to be ill-posed. This algorithm is based on the PSO algorithm with a random topology of links with the addition of genetic operators for crossover and mutation and the implementation of the evolution of links between swarm particles. In contrast to the conventional PSO algorithm, the crossover for particle coordinates and velocities is borrowed from the genetic algorithm. At the same time, two subsets are selected from the entire set of particles. The rules for updating velocities and positions are applied several times to the particles belonging to the "PSO subset" and they are ordered so that individuals with lower values of the target function belong to this subset, and the rest are replaced by the results of applying genetic operators to the elements of the second subset. In addition, in order to improve the efficiency of the algorithm, a crossover operator for the connections between particles is also introduced, which implements the evolution of the connections topology. The process is repeated until an acceptable solution is found.

The second approach also uses the surrogate optimization technique with all the nuances mentioned above, but the optimization is performed in a search space of reduced dimensionality, i.e. the latent space. Its dimensionality implies adjustments enabling to find a balance between the computational complexity and accuracy of the problem solution results. The dimensionality of the space is reduced by applying the PCA (Principal Component Analysis) method of linear data mapping into a new space of properties that are independent of each other, with a slight loss of information [31–34]. The transition to the latent space is realized by applying the SVD (Singular Value Decomposition) technique to the Gram matrix obtained from the training set, followed by the analysis of singular numbers and the selection of eigenvectors providing the largest variances in the new coordinate system. In this case, the metamodels have to be created in the latent space, in which the optimization is also performed using the target function of the form (3). After finding the solution, it is necessary to return to the original coordinate system. Owing to a rational regulated choice of the dimensionality of the latent search space, this hybrid approach leads to a significant reduction in the variables for the optimization algorithm, reducing the computation time without a significant loss of solution accuracy, which makes it very effective.

It should be noted that both methods require training on a large dataset containing information on electromagnetic measurements and the corresponding EC and MP profiles.

## 4. Inverse problem of profiles defining

### 4.1. Method of classical surrogate optimisation

The first step in solving the multivariate inverse problem of measuring of profiles of material properties by the classical surrogate optimization method is to create metamodels as proxy-models and carriers of apriori information about the TO. Using the algorithm for constructing surrogate models proposed by the authors in [22, 23, 29], metamodels were created taking into account the measurement conditions and possible changes in the ECP signal. To build the metamodels, a volumetric sample is designed for the DFCNN training at the points of the multidimensional DOE [35] based on the Sobol's $LP_\tau$-sequences, providing their high accuracy. This sample was obtained by calculation using the "exact" electrodynamic model [5, 19] and is presented in Table 1.

It should be borne in mind that, in addition to the basic (ideal) profiles of the EC and MP, their scattering within the technological tolerance $\delta T$, % on the TO surface is possible, where the change

Table 1. Total sample size of 8191 × 102 for creating metamodels

| № Profile | $Re(e_{mod})$ | $Im(e_{mod})$ | $\mu_1$ | $\mu_2$ | ... | $\mu_{51}$ | $\sigma_1$ | $\sigma_2$ | ... | $\sigma_{51}$ |
|---|---|---|---|---|---|---|---|---|---|---|
| 1 | –0.9697 | –1.697 | 1.087 | 1.345 | ⋯ | 26.097 | 8 771 549 | 8 367 573 | ⋯ | 2 073 403 |
| 2 | –0.9696 | –1.635 | 1.080 | 1.318 | ⋯ | 24.140 | 9 422 131 | 8 980 990 | ⋯ | 2 107 756 |
| 3 | –0.967 | –1.757 | 1.093 | 1.372 | ⋯ | 28.054 | 8 120 966 | 7 754 157 | ⋯ | 2 039 050 |
| 4 | –0.9432 | –1.683 | 1.077 | 1.305 | ⋯ | 23.161 | 7 795 675 | 7 447 448 | ⋯ | 2 021 873 |
| 5 | –0.9783 | –1.7 | 1.090 | 1.358 | ⋯ | 27.076 | 9 096 840 | 8 674 282 | ⋯ | 2 090 580 |
| ⋯ | ⋯ | ⋯ | ⋯ | ⋯ | ⋯ | ⋯ | ⋯ | ⋯ | ⋯ | ⋯ |
| 8 191 | –0.9676 | –1.802 | 1.100 | 1.399 | ⋯ | 30.011 | 7 808 166 | 7 459 226 | ⋯ | 2 022 533 |

in these parameters is of maximum importance. That is, when constructing a multidimensional DOE, the maximum change in the profiles of material properties within this tolerance was considered. Then the metamodels regarding, for example, the four influencing factors will have the form $e_{metamod} = F(\boldsymbol{\sigma}_{max}, \boldsymbol{\mu}_{max}, z, f)$, of which $\boldsymbol{\sigma}_{max} = var$, $\boldsymbol{\mu}_{max} = var$, $z = var$, $f = var$. Using the successful sets of $LP_\tau$-sequences calculated for a single hypercube [35], the groups of their combinations of two to nine factors were created. The resulting designs on the sequences were analyzed both by the centered CD and wrap-around WD discrepancies and the newest ones – mixed MD and weighted symmetric centered WSCD discrepancies [36, 37], which together make it possible to assess the homogeneity of the DOEs created on their basis.

In these studies, the authors limited themselves to the simplest case, where metamodels take into account only a change in two factors $e_{metamod} = F(\boldsymbol{\sigma}_{max}, \boldsymbol{\mu}_{max})$. For DOEs on $LP_\tau$-sequences $\xi_1$, $\xi_6$, a transition from a unit square to a rectangle of the real factor space was made by scaling from a unit square to a rectangle, taking into account that the material properties vary within the technological tolerance $\delta T = \pm 15\%$. The basic profile is the EC profile, the minimum and maximum values for which are $\sigma_{min} = 2 \cdot 10^6$ S/m, $\sigma_{max} = 9.2 \cdot 10^6$ S/m, and for the MP profile – $\mu_{min} = 1$, $\mu_{max} = 26.1$, respectively. Then, within the technological tolerance, the ranges of change in the EC parameters are $7.82 \cdot 10^6 \leq \sigma_{max} \leq 10.1 \cdot 10^6$ S/m; and the MP – $22.185 \leq \mu_{max} \leq 30.015$, with $\sigma_{min}$ and $\mu_{min}$ remaining unchanged. Other initial data required to create the DOE are as follows: the height of the ECP above the TO $z = 1 \cdot 10^{-3}$ m, the excitation current frequency $f = 2 \cdot 10^3$ Hz the thickness of the subsurface layer $D = 3 \cdot 10^{-4}$ m, which was subject to conditional division into $L = 51$ layers to obtain piecewise constant profiles of the material properties.

Within the specified limits of changes in material properties, we calculated the distribution of EC $\boldsymbol{\sigma}$ using the typical "exponent" approximation and the distribution of MP $\boldsymbol{\mu}$ using the "gaussian" approximation [4] for the number of DOE points $N_{profile} = 8\,191$, which corresponds to the number of profiles in the total sample. For example, the variants of some of the four profiles out of possible 8 191 cases of distributions of material properties in the subsurface TO layers calculated according to the created DOE, are shown in Fig. 3.

(a)                                                      (b)
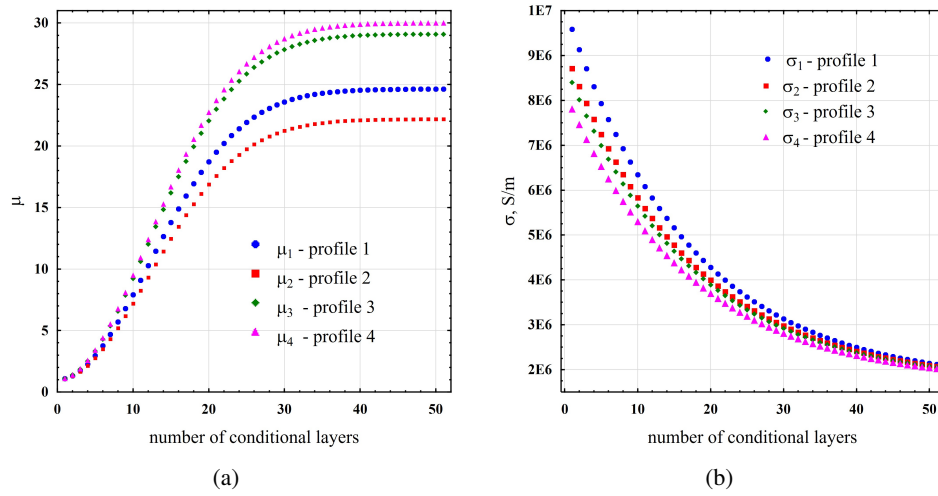
Fig. 3. Profiles of material properties in the subsurface layer of the TO for some of their cases: distribution of MP **μ** according to the typical "gaussian" profile (a); distribution of EC **σ** according to the typical "exponential" profile (b)

This type of analysis showed the feasibility of DFCNN usage with four hidden layers and the Levenberg–Marquardt learning method. The general structure of the selected MLPs is as follows: MLP-$n_1 - n_2 - n_3 - n_4$-1, where $n_1$, $n_2$, $n_3$, $n_4$ is the number of hidden neurons in each layer (Fig. 4).
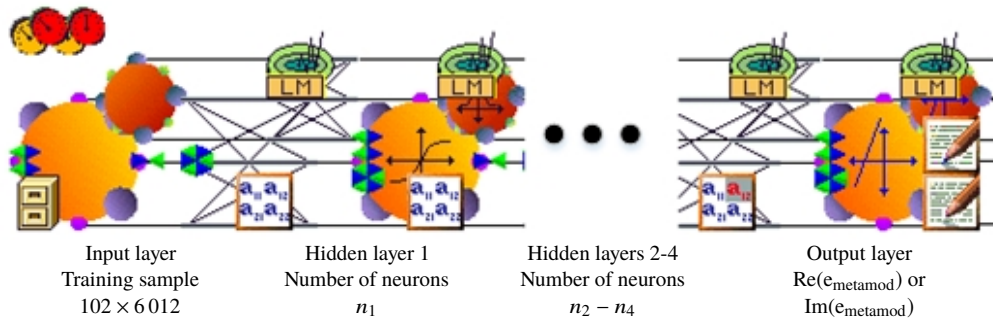


Fig. 4. General structure of neural network metamodels

As a result, we obtained the rMLP-30-30-20-10-1 networks for the real part of the EMF and the iMLP-25-25-20-10-1 networks for the imaginary part, respectively. The validity of the obtained metamodels was evaluated by the errors MAPE$_{metamod}$, % (Mean Absolute Percentage Error), separately for training, cross-validation, and test samples, the results of which are given in Table 2, and by analyzing the scatter plots (Fig. 5).

Table 2. Error of the approximation $MAPE_{metamod}$, % of obtained metamodels

| Metamodel | Training sample, $N_{traine} = 4\,206$ | Cross-validation sample, $N_{CV} = 903$ | Test sample, $N_{test} = 903$ | The total sample for training, $N = 6\,012$ |
|---|---|---|---|---|
| rMLP-30-30-20-10-1 | 0.00327 | 0.00323 | 0.00339 | 0.003296 |
| iMLP-25-25-20-10-1 | 0.01427 | 0.01506 | 0.01471 | 0.014487 |
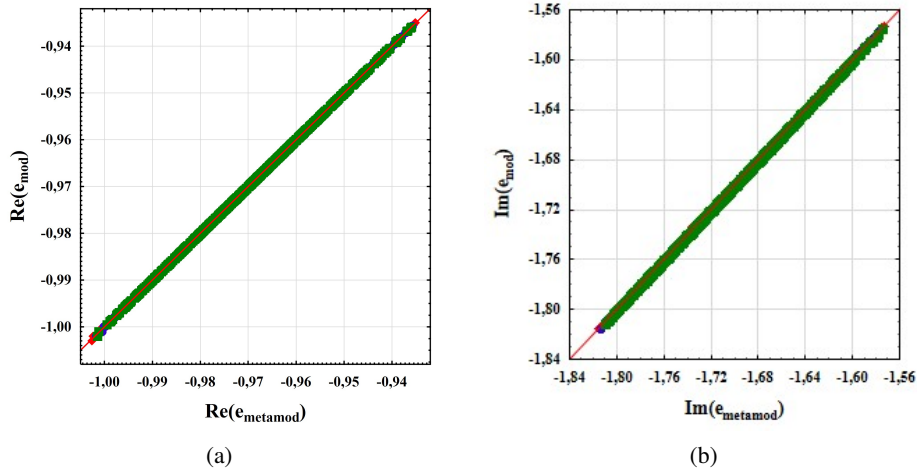


Fig. 5. Scatter diagrams of metamodels: rMLP-30-30-20-10-1 (a); iMLP-25-25-20-10-1 (b)

The verification of the obtained metamodels was carried out by checking the correctness of the reproducibility of the response surface in the entire modelling domain by a number of statistical indicators [38], the values of which are given in Tables 3 and 4.

The final stage of metamodels construction is to check their adequacy and informativeness. To verify the correspondence of the metamodels to the training data, their adequacy was determined by the Fisher criterion [38]. Thus, the obtained metamodel rMLP-30-30-20-10-1 has a Fisher's exponent value of $F_{102;5909}^{total} = 6.309 \cdot 10^6$, and the critical value of this criterion with a significance level of $\alpha = 5\%$ and the number of degrees of freedom $v_R = 5\,909$, $v_D = 102$ is

Table 3. Verification of the metamodel rMLP-30-30-20-10-1

| Variance components | Sum of squares | Middle square | Dispersion | Standard estimation error |
|---|---|---|---|---|
| regressions | $SS_D = 1.210734$ | $MS_D = 0.01186$ $v_D = 102$ | $\sigma_D^2 = 2.01419 \cdot 10^{-4}$ | $S_D = 0.01419221$ |
| residues | $SS_R = 1.116 \cdot 10^{-5}$ | $MS_R = 1.88 \cdot 10^{-9}$ $v_R = 5\,909$ | $\sigma_R^2 = 1.88 \cdot 10^{-9}$ | $S_R = 4.3458 \cdot 10^{-5}$ |
| general | $SS_T = 1.21074516$ | $MS_T = 2.014 \cdot 10^{-4}$ $v_T = 6011$ | $\sigma_T^2 = 2.01421 \cdot 10^{-4}$ | $S_T = 0.01419228$ |

Table 4. Verification of the metamodel iMLP-25-25-20-10-1

| Components variances | Sum of squares | Middle square | Dispersion | Standard estimation error |
|---|---|---|---|---|
| regressions | $\mathrm{SS}_D$ = 15.2868 | $\mathrm{MS}_D$ = 0.152811<br>$v_D$ = 102 | $\sigma_D^2$ = 0.00254313 | $\mathrm{S}_D$ = 0.050429 |
| residues | $\mathrm{SS}_R$ = 0.0004956 | $\mathrm{MS}_R$ = $8.38 \cdot 10^{-8}$<br>$v_R$ = 5909 | $\sigma_R^2$ = $8.38 \cdot 10^{-8}$ | $\mathrm{S}_R$ = $2.896 \cdot 10^{-4}$ |
| general | $\mathrm{SS}_T$ = 15.2873 | $\mathrm{MS}_T$ = 0.0025432<br>$v_T$ = 6011 | $\sigma_T^2$ = 0.0025432 | $\mathrm{S}_T$ = 0.05043 |

$F_{0.05;102;5909}^{\text{table}}$ = 1.2837, which satisfies the adequacy condition. For the metamodel iMLP-25-25-20-10-1, the adequacy condition for this criterion is also met, since $F_{102;5909}^{\text{total}}$ = $1.8 \cdot 10^6$. The model was tested for informativeness by calculating the coefficient of $R^2$ determination according to the data in Table 3 and Table 4 and testing the hypothesis of significance of this coefficient by Fisher's criterion. The coefficient of determination for both metamodels exceeds 0.99, which indicates their high informativeness. These coefficients are significant according to Fisher's criterion at the 5% significance level, since the condition of informativeness is met for both metamodels ($F_{102;5909}^{\text{total}}$ = $1.448 \cdot 10^6$).

The nonlinear inverse problem is formulated as follows: based on the measured value of $e_{\text{mes}}$ EMF of the ECP, it is necessary to determine the desired profiles of material properties consisting of 51 values of EC in the conditional layers of the TO and 51 values of MP, respectively, by means of global surrogate optimization in the full factor search space.

By averaging the results of a series of problem solutions, the reconstructed profiles of MP and EC along the depth of the subsurface layer were determined (Fig. 6). The parameters of the optimization algorithm are as follows: the number of swarm particles is 20; the inertial coefficient



(a)                                        (b)
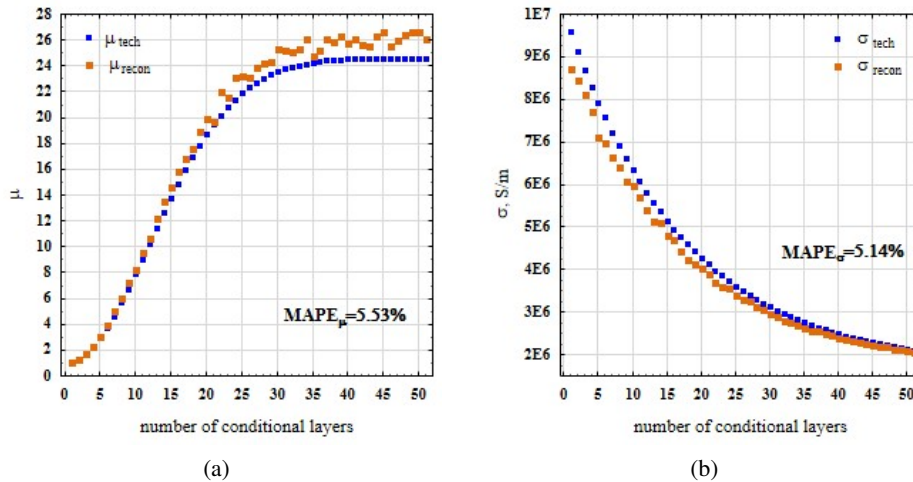
Fig. 6. Results of determining of MP and EC profiles

is 0.721; the cognitive and social coefficients are 1.193; the number of informants of other particles is 3; the number of offspring is 5; the mutation probability is 0.2 and the iteration step of genetic operators is 10.

Thus, the implementation of the first approach fails to give rather an acceptable result, which is explained by the significant difficulties in finding the optimum due to the "curse of dimensionality", even in the case of a small number of layers of conditional partitioning.

## 4.2. Hybrid surrogate optimization method

In order to reduce the dimensionality of the search space, the PCA method based on the SVD decomposition was used. As a result, 50 influential factors with eigenvalues greater than 1 were selected. Subsequently, metamodels were built according to the above scheme, where the training set is a matrix of parameters in a new latent factor space of size $N_{profile} \times n_{latent}$, where $n_{latent}$ is the number of variables in this space. The metamodels obtained in the space of reduced dimensionality for the real and imaginary parts of $e_{metamod}$ are given in Table 5, which shows the estimation of their training accuracy with the error $MAPE_{metamod}$, %. Figure 7 illustrates the histograms of distributions of absolute errors of the real and imaginary parts induced in the measuring turn of the ECP EMF, obtained by means of the created metamodels for the corresponding sample.

Table 5. Error of the approximation MAPE, % of metamodels in the latent space

| Metamodel | $MAPE_{metamod}$, % | | | |
|---|---|---|---|---|
| | Training sample, $N_{traine} = 4\,206$ | Cross-validation sample, $N_{CV} = 903$ | Test sample, $N_{test} = 903$ | The total sample for training, $N = 6\,012$ |
| rMLP-13-13-12-10-1 | 0.00914 | 0.01005 | 0.01023 | 0.00944 |
| iMLP-13-13-12-10-1 | 0.01302 | 0.01573 | 0.01586 | 0.01385 |

The inverse problem is formulated similarly to the previous definition: based on the measured value of $e_{mes}$ EMF of the ECP, it is necessary to determine the profiles of material properties consisting of 50 variables by means of global surrogate optimization in a new latent search subspace.

As in the previous case, we performed multistarts of the optimization algorithm and obtained fourteen solutions for the technological profiles of the MP and EC. At the same time, the parameters of the optimization algorithm remained unchanged, as in the previous method. These actions are performed for three EMF test measurement cases. After that, we returned to the original factor space in order to obtain the actual profiles. Table 6 shows the obtained values of MAPE errors for all individual solutions of $\boldsymbol{\mu}$ and $\boldsymbol{\sigma}$. Table 7 shows the values of the MP technological profile $\boldsymbol{\mu}_{tech}$ and the reconstructed $\boldsymbol{\mu}_{recon}$ for the two test measurements, obtained by averaging of the calculations, as well as the value of the relative error at each point of the profile $\delta_i$, %. The same, but for the profile of the EC, is given in Table 8.
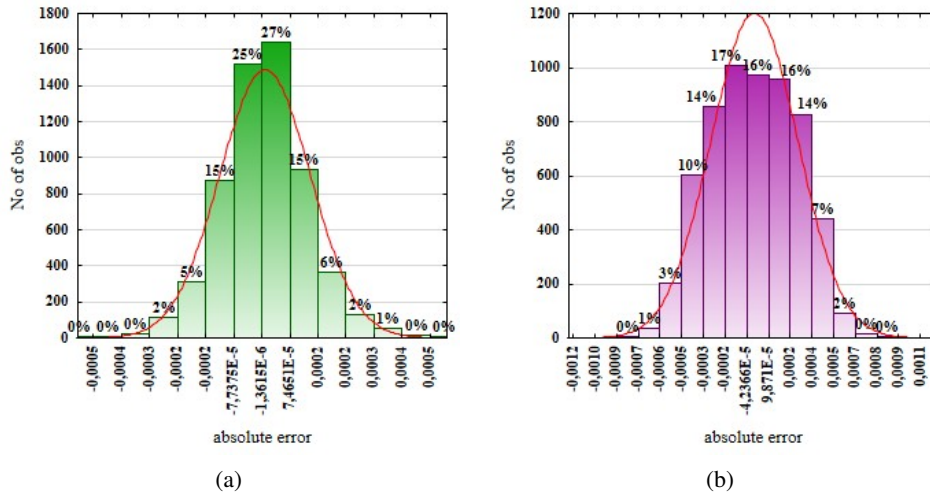
Fig. 7. Histograms of the distribution of absolute errors of the real and imaginary parts induced in the measuring turn of the ECP EMF for metamodels: rMLP-13-13-12-10-1 (a); iMLP-13-13-12-10-1 (b)

Table 6. Error values MAPE, % for the reconstructed profiles of the MP and EC

| № start | MAPE, % | | | | | |
|---|---|---|---|---|---|---|
| | **EMF test measurement 1** | | **EMF test measurement 2** | | **EMF test measurement 3** | |
| | $Re(e_{mes}) = -0.9739$ $Im(e_{mes}) = -1.637$ | | $Re(e_{mes}) = -0.9749$ $Im(e_{mes}) = -1.762$ | | $Re(e_{mes}) = -0.9648$ $Im(e_{mes}) = -1.627$ | |
| | μ | σ | μ | σ | μ | σ |
| 1 | 2.194 | 0.701 | 1.344 | 2.804 | 2.174 | 0.819 |
| 2 | 1.97 | 1.29 | 0.999 | 2.029 | 0.416 | 0.769 |
| 3 | 2.601 | 2.086 | 1.275 | 2.758 | 1.964 | 0.342 |
| 4 | 2.978 | 1.315 | 1.414 | 2.695 | 0.808 | 1.368 |
| 5 | 4.154 | 2.98 | 1.543 | 3.924 | 1.566 | 1.748 |
| . . . | . . . | . . . | . . . | . . . | . . . | . . . |
| 10 | 0.901 | 0.578 | 1.452 | 0.829 | 1.865 | 0.906 |
| 11 | 1.256 | 1.453 | 1.469 | 1.69 | 1.112 | 1.427 |
| 12 | 1.018 | 0.228 | 1.79 | 2.404 | 1.985 | 1.798 |
| 13 | 0.679 | 0.186 | 2.03 | 0.634 | 3.964 | 2.603 |
| 14 | 0.318 | 0.769 | 1.047 | 0.985 | 0.407 | 0.825 |

Table 7. Values of the technological and reconstructed MP profiles

| № conditional layer | EMF test measurement 1 $\mathrm{Re}(e_{\mathrm{mes}}) = -0.9739$ $\mathrm{Im}(e_{\mathrm{mes}}) = -1.637$ | | | EMF test measurement 2 $\mathrm{Re}(e_{\mathrm{mes}}) = -0.9749$ $\mathrm{Im}(e_{\mathrm{mes}}) = -1.762$ | | |
|---|---|---|---|---|---|---|
| | Profile $\mu_{\mathrm{tech}}$ | Profile $\mu_{\mathrm{recon}}$ | Relative error, $\delta_i$, % | Profile $\mu_{\mathrm{tech}}$ | Profile $\mu_{\mathrm{recon}}$ | Relative error $\delta_i$, % |
| 1 | 1.082 | 1.087 | 0.5395 | 1.097 | 1.104 | 0.6223 |
| 2 | 1.325 | 1.328 | 0.2333 | 1.386 | 1.405 | 1.3664 |
| 3 | 1.725 | 1.728 | 0.2225 | 1.861 | 1.881 | 1.0654 |
| 4 | 2.273 | 2.278 | 0.2093 | 2.516 | 2.534 | 0.8414 |
| … | … | … | … | … | … | … |
| 48 | 24.624 | 24.666 | 0.1717 | 29.085 | 29.159 | 0.2570 |
| 49 | 24.626 | 24.668 | 0.1717 | 29.087 | 29.162 | 0.2570 |
| 50 | 24.628 | 24.670 | 0.1717 | 29.089 | 29.164 | 0.2570 |
| 51 | 24.629 | 24.671 | 0.1717 | 29.091 | 29.166 | 0.2570 |

Table 8. Values of the technological and reconstructed EC profiles

| № conditional layer | EMF test measurement 1 $\mathrm{Re}(e_{\mathrm{mes}}) = -0.9739$ $\mathrm{Im}(e_{\mathrm{mes}}) = -1.637$ | | | EMF test measurement 2 $\mathrm{Re}(e_{\mathrm{mes}}) = -0.9749$ $\mathrm{Im}(e_{\mathrm{mes}}) = -1.762$ | | |
|---|---|---|---|---|---|---|
| | Profile $\sigma_{\mathrm{tech}}$ | Profile $\sigma_{\mathrm{recon}}$ | Relative error, $\delta_i$, % | Profile $\sigma_{\mathrm{tech}}$ | Profile $\sigma_{\mathrm{recon}}$ | Relative error, $\delta_i$, % |
| 1 | 9.584777 | 9.6513676 | 0.6948 | 8.397073 | 8.43036 | 0.3964 |
| 2 | 9.134344 | 9.1973851 | 0.6902 | 8.014491 | 8.04763 | 0.4135 |
| 3 | 8.709643 | 8.7693371 | 0.6854 | 7.653764 | 7.68677 | 0.4312 |
| 4 | 8.309205 | 8.365743 | 0.6804 | 7.313644 | 7.34652 | 0.44952 |
| … | … | … | … | … | … | … |
| 48 | 2.196699 | 2.2050656 | 0.3809 | 2.12188 | 2.1528 | 1.4570 |
| 49 | 2.168324 | 2.1764671 | 0.3756 | 2.097779 | 2.12869 | 1.4734 |
| 50 | 2.14157 | 2.1495023 | 0.3704 | 2.075055 | 2.10595 | 1.4891 |
| 51 | 2.116344 | 2.1240776 | 0.3654 | 2.053629 | 2.08445 | 1.5043 |

## 5. Discussion

Two methods for solving the inverse problem formulated in terms of optimization are proposed in this article, which systematically combine physical measurements and the mathematical apparatus for processing the information received by the probe, adequate for incorrectly set tasks. The methods are implemented in the form of algorithmic and software reconstruction of profiles, which together constitute the defining achievements of the study. To minimize the target function a heuristic bionic hybrid algorithm for finding the global extremum is used. The quadratic target function includes the components calculated using computationally efficient metamodels serving as carriers of apriori accumulated information about the TO and accurately approximate the response surface originally specified by the electrodynamic model. Metamodels are created on two really significant deep fully connected neural networks, which provide the above properties, in particular: for the first method – MAPE$_{\text{metamod}}$ is 0.003296% and 0.014487%, respectively, for the real and imaginary parts of the EMF; for the second MAPE$_{\text{metamod}}$ is 0.00944% and 0.01385%, respectively, for the real and imaginary parts of the EMF. At the same time, the simplest case was used: metamodels take into account only changes in two factors $\boldsymbol{\sigma}_{\text{max}}$ and $\boldsymbol{\mu}_{\text{max}}$. The adequacy and informative value of the constructed metamodels of measurements by surface ECP has been proved. According to Fischer's criterion, both metamodels are adequate with a significance level of 5%, where the criterion indicator is no worse than $F_{102;5909}^{\text{total}} = 1.8 \cdot 10^6$, and informative with a coefficient of determination of more than 0.99. Numerical simulations demonstrate the adequacy of both methods with an acceptable profile reconstruction accuracy. Thus, for the first method, a series of twenty-one solutions to the nonlinear inverse problem by means of surrogate optimization obtained reconstructed profiles of MP and EC along the depth of the subsurface layer, which together provide the maximum coincidence of the $e_{\text{mod}}$ value with the measured $e_{\text{mes}}$. For the obtained solutions, the error range MAPE, % is from 4.25% to 8.92%. By averaging the results of all solutions, the reconstructed profiles of the MP and EC were determined, with the MP profile obtained with error MAPE, % – 5.53% and 5.14% for the EC profile (Fig. 6). Thus, the implementation of the first approach gives a not very acceptable result, which is explained by the significant difficulty of finding the optimum due to the "curse of dimensionality", even in the case of a small number of layers of conditional partitioning. The implementation of the second method yields error MAPE, % that does not exceed 0.352% and error MAPE, % of 0.96% for the MP and EC profiles, respectively.

A significant difference between the proposed methods is the measurability of the factor space where the optimization algorithm is implemented. Unlike the first, the second original method takes advantage of the surrogate optimization in the search space of reduced dimensionality. In this case, the dimensionality of the space is controlled by a researcher and is much smaller than the original one, which can approximately constitute 40%. Thus, this provides a possibility to significantly reduce the number of variables defining the profiles, with all the consequences: twice reduced computation time, simplified conditions for finding the extremum with an indirect positive effect on the accuracy of its finding. To transform the search space, the PCA principal component method is applied, which ensures minimal loss of information and a balance between a computational complexity and accuracy of the results.

## 6. Conclusions

The following conclusions can be drawn regarding the research results. One of the most important features of the proposed methods for measuring the profiles of material properties of planar TO by eddy-current probes is the application of the latest surrogate strategies in combination

with modern global optimization techniques, which allows improving the efficiency and reducing the resource consumption of problem solutions, and ensuring a balance between computational complexity and accuracy of the obtained results. It was achieved by creating high-performance metamodels based on real-valued deep fully-connected neural networks. In addition, the high accuracy of the approximation of the multidimensional response surface is ensured by performing calculations according to a computer homogeneous design of experiment with a low weighted symmetrized centered discrepancy. We present the results of numerical experiments performed in the search spaces of full and reduced dimensions, the latter of which is obtained by linear transformations using the principal component method. The methods were verified by simulating the measurements on synthetically generated data not used in training, testing, and verification of metamodels, but known in advance. The results obtained prove to be sufficiently accurate in reconstructing the profiles of electrical conductivity and magnetic permeability of planar test objects.

## References

[1] Xia Z., Huang R., Chen Z., Yu K., Zhang Z., Salas-Avila J.R., Yin W., *Eddy current measurement for planar structures*, Sensors, vol. 22, no. 22, 8695 (2022), DOI: 10.3390/s22228695.

[2] Lu M., *Forward and inverse analysis for non-destructive testing based on electromagnetic computation methods*, PhD Thesis, The University of Manchester (United Kingdom) (2018).

[3] Campbell S.D., Sell D., Jenkins R.P., Whiting E.B., Fan J.A., Werner D.H., *Review of numerical optimization techniques for meta-device design*, Optical Materials Express, vol. 9, no. 4, pp. 1842–1863 (2019), DOI: 10.1364/OME.9.001842.

[4] Halchenko V.Y., Tychkov V.V., Storchak A.V., Trembovetska R.V., *Reconstruction of surface radial profiles of the electrophysical characteristics of cylindrical objects during eddy current measurements with a priori data*, The selection formation for the surrogate model construction, Ukrainskyi Metrolohichnyi Zhurnal, no. 1, pp. 35–50 (2020), DOI: 10.24027/2306-7039.1.2020.204226.

[5] Trembovetska R., Halchenko V., Bazilo C., *Inverse multi-parameter identification of plane objects electrophysical parameters profiles by eddy-current method*, In Smart Technologies in Urban Engineering: Proceedings of STUE-2022, Cham: Springer International Publishing, pp. 202–212 (2022), DOI: 10.1007/978-3-031-20141-7_19.

[6] Tesfalem H., Hampton J., Fletcher A.D., Brown M., Peyton A.J., *Electrical resistivity reconstruction of graphite moderator bricks from multi-frequency measurements and artificial neural networks*, IEEE Sensors Journal, vol. 21, no. 15, pp. 17005–17016 (2021), DOI: 10.1109/JSEN.2021.3080127.

[7] Hampton J., Fletcher A., Tesfalem H., Peyton A., Brown M., *A comparison of non-linear optimisation algorithms for recovering the conductivity depth profile of an electrically conductive block using eddy current inspection*, NDT & E International, vol. 125, 102571 (2022), DOI: 10.1016/j.ndteint.2021.102571.

[8] Tesfalem H., Peyton A.J., Fletcher A.D., Brown M., Chapman B., *Conductivity profiling of graphite moderator bricks from multifrequency eddy current measurements*, IEEE Sensors Journal, vol. 20, no. 9, pp. 4840–4849 (2020), DOI: 10.1109/JSEN.2020.2965201.

[9] Xu J., Wu J., Xin W., Ge Z., *Measuring ultrathin metallic coating properties using swept-frequency eddy-current technique*, IEEE Transactions on Instrumentation and Measurement, vol. 69, no. 8, pp. 5772–5781 (2020), DOI: 10.1109/tim.2020.2966359.

[10] Xu J., Wu J., Xin W., Ge Z., *Fast measurement of the coating thickness and conductivity using eddy currents and plane wave approximation*, IEEE Sensors Journal, vol. 21, no. 1, pp. 306–314 (2020), DOI: 10.1109/jsen.2020.3014677.

[11] Huang P., Zhao J., Li Z., Pu H., Ding Y., Xu L., Xie Y., *Decoupling conductivity and permeability using sweep-frequency eddy current method*, IEEE Transactions on Instrumentation and Measurement, vol. 72, pp. 1–11 (2023), DOI: 10.1109/tim.2023.3242017.

[12] Hampton J., Tesfalem H., Fletcher A., Peyton A., Brown M., *Reconstructing the conductivity profile of a graphite block using inductance spectroscopy with data-driven techniques*, Insight-Non-Destructive Testing and Condition Monitoring, vol. 63, no. 2, pp. 82–87 (2021), DOI: 10.1784/insi.2021.63.2.82.

[13] Yi Q., Tian G.Y., Malekmohammadi H., Laureti S., Ricci M., Gao S., *Inverse reconstruction of fibre orientation in multilayer CFRP using forward FEM and eddy current pulsed thermography*, NDT & E International, vol. 122, 102474 (2021), DOI: 10.1016/j.ndteint.2021.102474.

[14] Halchenko V.Y., Storchak A.V., Trembovetska R.V., Tychkov V.V., *The creation of a surrogate model for restoring surface profiles of the electrophysical characteristics of cylindrical objects*, Ukrainian Metrological Journal, no. 3, pp. 27–35 (2020), DOI: 10.24027/2306-7039.3.2020.216824.

[15] Bowler N., *Eddy-Current Nondestructive Evaluation*, Springer New York (2019).

[16] Lei Y.Z., *General series expression of eddy-current impedance for coil placed above multi-layer plate conductor*, Chinese Physics B, vol. 27, no. 6, 060308 (2018), DOI: 10.1088/1674-1056/27/6/060308.

[17] Uzal E., *Theory of eddy current inspection of layered metals*, Iowa State University (1992).

[18] Zhang J., Yuan M., Xu Z., Kim H.J., Song S.J., *Analytical approaches to eddy current nondestructive evaluation for stratified conductive structures*, Journal of Mechanical Science and Technology, vol. 29, pp. 4159–4165 (2015), DOI: 10.1007/s12206-012-0911-8.

[19] Theodoulidis T.P., Kriezis E.E., *Eddy current canonical problems (with applications to nondestructive evaluation)*, Tech Science Press (2006).

[20] Halchenko V.Y., Trembovetska R.V., Bazilo C.V., Tychkova N.B., *Computer simulation of the process of profiles measuring of objects electrophysical parameters by surface eddy current probes*, in Lecture Notes on Data Engineering and Communications Technologies: Proceedings of ITEST 2022, Springer Cham, vol. 178, pp. 411–424 (2023), DOI: 10.1007/978-3-031-35467-0_25.

[21] Jiang P., Zhou Q., Shao X., *Surrogate model-based engineering design and optimization*, in: Surrogate Model-Based Engineering Design and Optimisation, Springer Tracts in Mechanical Engineering, Springer, Singapore (2020).

[22] Halchenko V.Y., Trembovetska R.V., Tychkov V.V., *Surrogate synthesis of frame eddy current probes with uniform sensitivity in the testing zone*, Metrology and Measurement Systems, vol. 28, no. 3, pp. 551–564 (2021), DOI: 10.24425/mms.2021.137128.

[23] Halchenko V.Y., Trembovetska R.V., Tychkov V.V., *Surrogate synthesis of excitation systems for frame tangential eddy current probes*, Archives of Electrical Engineering, vol. 70, no. 4, pp. 743–757 (2021), DOI: 10.24425/aee.2021.138258.

[24] Kuznetsov B., Bovdui I., Nikitina T., Kolomiets V., Kobylianskyi B., *Surrogate synthesis of system of active shielding of magnetic field generated by group of overhead power lines*, in IEEE EUROCON 2021-19th International Conference on Smart Technologies, pp. 381–384 (2021).

[25] Fang K., Liu M.Q., Qin H., Zhou Y.D., *Theory and Application of Uniform Experimental Designs*, Springer, Singapore (2018).

[26] Xu Q., Ping H., Lin D.K.J., Liu M.-Q., Zhou Y., *Theory and application of uniform designs*, Scientia Sinica Mathematica, vol. 50, no. 5, 561 (2020), DOI: 10.1360/SSM-2020-0065.

[27] Wang Y., Sun F., Xu H., *On design orthogonality, maximin distance, and projection uniformity for computer experiments*, Journal of the American Statistical Association, vol. 117, iss. 537, pp. 375–385 (2022), DOI: 10.1080/01621459.2020.1782221.

[28] Halchenko V.Y., Yakimov A.N., Ostapuschenko D.L., *Global optimum search of functions using multia-gent swarm optimisation hybrid with evolutionary composition formation of population*, Information Technology (in Russian), no. 10, pp. 9–16 (2010).

[29] Halchenko V.Y., Trembovetska R.V., Tychkov V.V., Storchak A.V., *Nonlinear surrogate synthesis of the surface circular eddy current probes*, Przegląd Elektrotechniczny, no. 9, pp. 76–82 (2019), DOI: 10.15199/48.2019.09.15.

[30] Kuznetsov B., Bovdui I., Nikitina T., *Optimal design of system of active shielding of magnetic field generated by overhead power lines*, in 2021 IEEE 16th International Conference on the Experience of Designing and Application of CAD Systems (CADSM), pp. 4–1 (2021).

[31] Géron A., *Hands-On Machine Learning with Scikit-Learn, Keras, and TensorFlow*, O'Reilly Media, Inc. (2022).

[32] Géron A., *Deep Learning with TensorFlow*, Dunod (2017).

[33] Raschka S., *Machine learning* (2017).

[34] Wang J., Zhou J., Chen X., *Data-driven fault detection and reasoning for industrial monitoring*, Springer Nature (2022).

[35] Halchenko V.Y., Trembovetska R.V., Tychkov V.V., Storchak A.V., *The construction of effective multidimensional computer designs of experiments based on a quasi-random additive recursive Rd–sequence*, Applied Computer Systems, vol. 25, no. 1, pp. 70–76 (2020), DOI: 10.2478/acss-2020-0009.

[36] Ke X., Zhang R., Ye H.J., *Two-and three-level lower bounds for mixture $L_2$-discrepancy and construction of uniform designs by threshold accepting*, Journal of Complexity, vol. 31, no. 5, pp. 741–753 (2015), DOI: 10.1016/j.jco.2015.01.002.

[37] He L., Qin H., Ning J., *Weighted symmetrized centered discrepancy for uniform design*, Communications in Statistics-Simulation and Computation, vol. 51, no. 8, pp. 1–11 (2020), DOI: 10.1080/03610918.2020.1744063.

[38] Douglas C.M., *Design and Analysis of Experiments*, Wiley, London (2009).